Perturbed angular correlation study of ^{181}Ta-doped $PbTi_{1-x}Hf_xO_3$ compounds

R.E. Alonso , A.R. López García , M.A. de la Rubia , J. De Frutos

A B S T R A C T

In this work, the hyperfine quadrupole interaction at Ta-doped $PbTi_{1-x}Hf_xO_3$ polycrystalline samples is studied for the first time. Powders with $x=0.25$, 0.50 and 0.75 were prepared and characterized by X-ray diffraction analysis. Perturbed Angular Correlation (PAC) analyses were done as a function of temperature, using low concentration ^{181}Ta nuclei as probes. In the ferroelectric and paraelectric phases of these compounds two sites were occupied by the probes. For each site the quadrupole frequency, asymmetry and relative distribution width parameters were obtained as a function of temperature above and below the Curie temperature (T_C). One of these sites was assigned to the regular Ti–Hf site, while the other one was assigned to some kind of defect. The behavior of the hyperfine parameters as a function of temperature was analyzed in terms of a recent published phase diagram and the presence of disorder below and above T_C. For the three compositions measured, the obtained hyperfine parameters present discontinuities which correspond to the ferroelectric–paraelectric phase transition. In both phases it was found broad frequency distributed interactions. The disorder in the electronic distribution would be responsible for the broad line width of the hyperfine interaction.

1. Introduction

Perovskite-type compounds with chemical formula ABO_3 have been the subject of several studies due to their fascinating electrical and magnetic properties such as ferro and antiferroelectricity, superconductivity, piezoelectricity and colossal magneto resistance. These compounds are suitable for a wide variety of applications in microelectronics. Performing partial substitutions of A and/or B by homovalent or heterovalent cations (A′ and B′), solid solutions with general formula $A_yA'_{1-y}B_xB'_{1-x}O_3$ with $0<x$, $y<1$ are obtained. These substitutions can change the physical properties of the materials, making these compounds suitable for materials design. In these oxides A and A′ and B and B′ are randomly distributed in their corresponding sites. Experiments show that these solid solutions are not mixtures of simple perovskites. At high temperatures, perovskite-type compounds present cubic symmetry, with the B (and B′) cation in the center of the cubic unit cell, the A (or A′) cation in the vertices of the cube and the O anions at the center of the faces forming a regular octahedron that encloses the B cations. As the temperature decreases, these compounds exhibit phase transitions to structures of lower symmetry, and their phase diagrams are strongly dependent on the characteristics of the A, A′, B and B′ elements. In these phase transitions, the atomic displacements from their ideal positions in the cubic structure are relatively small [1–6]. It has been observed that these materials can contain oxygen vacancies [7]. Their content is strongly dependent on the preparation method and on the subsequent thermal treatments. Some macroscopic physical properties are directly related with such defects.

$PbTi_{1-x}Hf_xO_3$ (PTH) family of compounds presents an important interest due to its ferroelectric properties. It is a particular case of $A_yA'_{1-y}B_xB'_{1-x}O_3$ with $y=1$ and the Ti and Hf atoms are randomly distributed in the B–B′ site. Taking into account the valences and chemical properties of the B and B′ cations, this family of compounds is expected to be similar to the highly utilized $PbZr_xTi_{1-x}O_3$ (PZT) in microelectronics. Regarding the pure constituent oxides, $PbTiO_3$ (PT) is ferroelectric at room temperature (RT) with tetragonal P4mm structure and lattice constants $a=3.9036(1)$ Å and $c=4.1440(2)$ Å [8,9]. The other binary oxide $PbHfO_3$ (PH) in the same conditions is antiferroelectric and has an orthorhombic Pbam structure with $a=4{,}150(1)$ Å, $b=3.919(1)$ Å and $c=4.114(1)$ Å [8,10,11].

It has been observed that almost all the mixtures $ABB'O_3$ perovskites have the same crystalline structure at RT as that of

the major proportion ABO_3 or $AB'O_3$ simple perovskite forming the alloy has. In PTH the mix of the primary oxides PT and PH produces at room pressure a tetragonal structure for Ti rich compositions. But for $x > 0.5$ and below the Curie temperature (T_C) a rhombohedral structure that is not present in any of the two constituent oxides was observed [12]. At $x=0.5$, the coexistence of a monoclinic structure that is neither present in the pure oxides nor together with the rhombohedral structure has been reported [14]. The phase diagram of PTH has been previously studied [12–14]. For its determination, different experimental techniques were employed (Impedance Spectroscopy, Differential Scanning Calorimetric, Thermo Gravimetric Analysis, X-ray absorption fine structure (XAFS), X-ray and Neutron Powder Diffraction) [12–17]. In the literature there are some differences in the temperature at which the phase transitions occur. The different results were obtained by different experimental conditions and thermal treatments. Moreover, the different methods of sample preparation can affect the grain size, its distribution, and the corresponding phase stability.

In different studies of perovskite-type compounds, the phase stability and the transition temperatures were analyzed in terms of the hyperfine interaction parameters of probe atoms using Perturbed Angular Correlations spectroscopy (PAC) [18–24]. The Electric Field Gradient tensor (EFG) is a very sensitive physical quantity that strongly depends on the charge distribution in the close neighbor of the probe. Thus, the analysis of the temperature dependence of the hyperfine parameters can detect tiny changes of the surrounding charge distribution at a nanoscopic range. So, PAC spectroscopy has been demonstrated to be a suitable technique to sense the presence of vacancies, disorder and charge transfer processes, together to allow the determination of phase transition temperatures. In an ideal cubic perovskite structure, the EFG at the B site should vanish by symmetry. However, in real compounds two kinds of finites perturbations on probes were detected: static, asymmetric and disordered electric nuclear quadrupole interactions (NQI) [21,22] and nuclear spin relaxations [25]. In a recent work the origin of the static fields as a result of the presence of oxygen vacancies and different degrees of covalence of the B–O and B′–O bonds was explained [22]. On the other hand the origin of the nuclear spin relaxation processes in ABO_3 compounds has been related with other different complex dynamic processes due to decaying probe "after effects" and vacancies mobility. As the PTH materials are nonmagnetic, the charge density is manifested through the EFG measured at the B–B′ sites. PAC spectroscopy can accomplish this goal if one succeeds in placing a suitable probe at this site.

In this contribution we present the study the electric hyperfine interaction measured by PAC spectroscopy at ^{181}Ta probes in polycrystalline samples of $PbTi_{1-x}Hf_xO_3$ for $x=0.25$, 0.50 and 0.75. The choice and preparation of ^{181}Hf probes via neutron capture warrants unambiguous B-site location of the daughter ^{181}Ta in the matrix. This opens the possibility to follow the phase transitions and the nanoscopic effects of B–B′ substitution at a well-defined lattice site. By measuring the temperature dependence of the EFG we also hope to gain information about the sample defect structure because such structures often lead to additional contributions to the PAC perturbation function.

2. Sample preparation

The different compounds of $PbTi_{1-x}Hf_xO_3$ were prepared by conventional ceramic route of mixing the corresponding oxides. Powder raw materials with a purity of 98% for PbO and TiO_2 and HfO_2 (with 2% ZrO_2) were mixed thoroughly in a high speed mill for 10 min in ethanol with ZrO_2 balls. The powders were dried at 60 °C and sieved at 63 μm, followed with a solid state reaction at 850 °C for 4 h where the material was synthesized. After that, the compounds were milled again in the same conditions and dried, after which a binder was added. Pellets of 1 mm in thickness and 10 mm in diameter were axially pressed at 80 MPa. The calcination of the binder was carried out at 600 °C for 1 h. And finally, the samples were sintered at 1250 °C for 4 h with a heating rate of 3 °C/min. The difficulty in the preparation of PTH ceramics arises from the high volatility of PbO during sintering. In order to minimize the PbO volatilization, the pellets were sintered in a Pb-rich atmosphere by carrying out the sintering in a closed system by means of a double alumina crucible setup where the pellets were placed on platinum sheet with a buffer powder of $PbZrO_3$ and ZrO_2 that was 5% of the total weight of the samples. The joint between alumina crucibles was sealed with ZrO_2 powder. The weight change of the samples was less than 2%. To eliminate layers on top and bottom where the Pb loss is more noticeable, the pellets were polished with a SiC sandpaper. After that, the surfaces were tan in color and X-ray diffraction analysis (XRD) of the surfaces showed only the perovskite phase. Even with the Pb evaporation effect, all samples showed a very high density, usually >95% of the nominal bulk density, determined by the Arquímedes dipping method. Using this procedure all samples showed even higher densities after the elimination of Pb-poor surfaces. On these surfaces the presence of HfO_2 and TiO_2 should be proportional to the Pb-loss. The pellets used in the electrical and thermal characterization do not show the presence of these oxides in the X-ray characterization of the polished surface. Fig. 1 shows the final XRD spectra at RT for each composition after the whole process. In them no traces of other phases or compounds can be observed. The thermal evolution of the mixtures was controlled by XRD analysis at RT. This procedure showed that all samples treated at 850 °C–4 h the perovskite structure is formed and there is no signal left of the starting oxides. The diffraction patterns showed that the compounds were almost completely crystallized after the second heating at 600 °C. The spectra were fitted following the results obtained in previous detailed works (neutron diffraction spectroscopy and XAFS, Refs. [14,17]):tetragonal P4mm for $x=0.25$ ($a=3.9520_3$ Å, $c=4.1436_8$ Å), rhombohedral hexagonal R3c ($a=5.7231_5$ Å and $c=14.1316_2$ Å) and monoclinic Cm ($a=5.702_7$ Å, $b=5.6922_8$ Å and $c=4.1040_5$ Å) for $x=0.50$, and rhombohedral for $x=0.75$ ($a=4.1392_4$ and $\alpha=89.683_5°$.

For PAC spectroscopy the ^{181}Ta probe at the Hf–Ti site was used. It was produced by thermal neutrons irradiation of ^{180}Hf already contained in the sample as one of the natural isotopes of

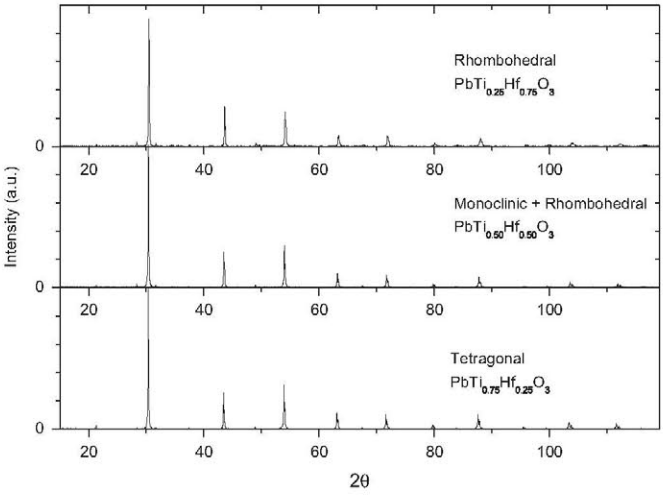

Fig. 1. XRD spectra of $PbTi_{1-x}Hf_xO_3$ at RT for $x=0.25$, 0.50 and 0.75 after the sample preparation process.

this metal. The samples were irradiated with a neutron flux of 2×10^{13} n/cm^2 s^{-1} in the Centro Atómico Ezeiza reactor (Comisión Nacional de Energía Atómica, *Ezeiza*, Argentina) for approximately 7 h at 60 °C in order to obtain an activity of 300 μCi. The ^{181}Ta concentration obtained remains lower than ppm. This extremely small impurity concentration is expected not to affect the bulk properties of the pure material. As the transition from ^{181}Hf to ^{181}Ta is done via a β^- decay, and the start level of the 133–482 KeV cascade has a half-life large enough to allow the necessary electronic reorientation prior to the beginning of the cascade (17.8 μs), no "after effects" are expected to be observed with this probe [26]. Moreover, it must be emphasized that the detected NQI reflect the local structure around Ta, not Hf. This fact does not depend on the compound in which the probe is, but in the probe itself. Under this assumption several EFG in different systems were correctly predicted [27].

3. PAC spectroscopy

The angular correlation function of a gamma–gamma cascade $W(\theta, t)$ that describes the interaction between the intermediate state nuclear quadrupole moment Q and the electric field gradient is given by

$$W(\theta,t) = 1 + A_{22}G_{22}(t)P_2(\cos\theta) + \ldots \quad (1)$$

where $G_{22}(t)=\Sigma f_s G^s_{22}(t)$, f_s is the fraction of nuclei perturbed at site s and $G^s_{22}(t)$ the perturbation fraction corresponding to this site. The $P_K(\cos\theta)$'s are the Legendre polynomials of rank K and θ the angle between both gamma rays. The A_{KK} are known coefficients depending on all spin quantum numbers involved in the cascade [28].

The EFG tensor which interacts with the nuclear quadrupole moment can be characterized by its maximal component V_{zz} and the asymmetry parameter η

$$\eta = (V_{xx}-V_{yy})/V_{zz}$$

where the principal axes are chosen in such a way that

$$|V_{yy}| \le |V_{xx}| \le |V_{zz}|$$

with these definitions $0 \le \eta \le 1$.

A static electric quadrupole interaction acting on nuclear state with spin $I=5/2$ is represented by

$$G_{22}(t) = \sigma_{20} + \Sigma\sigma_{2n}\cos(\omega_n t)\exp(-\omega_n\delta t) \quad (2)$$

where the sum runs from 1 to 3. The ω_n are related to the energy splitting produced by the static quadruple interaction and satisfy $\omega_1+\omega_2=\omega_3$. These frequencies depend on the quadruple frequency $\omega_Q=e^2QV_{zz}/[4I(2I-1)\hbar]$ and η. The σ_{2k} are functions only of the asymmetry parameter. For $I=5/2$ they are listed in Ref. [28]. Finally, δ is the line width that describes the disorder close to the probes and is represented by the Lorentzian distribution function.

For ^{181}Ta, $Q=2.53\times10^{-24}$ cm^2 is the quadrupole moment of the intermediate nuclear state of the 133–482 keV gamma–gamma cascade whose half life is 10.6 ns [29]. The EFG components are related to the charge density $\rho(r)$ close to probes nucleus by

$$V_{ij} = (1/4\pi\varepsilon_0)\int (r_i r_j - \delta_{ij}r^2)r^{-5}\rho(r)d\nu \quad (3)$$

where r represents the position with respect to the probe nucleus.

4. Experimental setup and data fit

The time spectra were measured with a two CsF detector spectrometer, storing coincidence data at 90°, 180° and 270°. The apparatus has a resolution time of ≈ 1 ns for the gamma–gamma cascade of ^{181}Ta. The coincidence spectra were obtained after an accumulation time of 1 day or more for every temperature. The anisotropy vs. time or spin precession curve is obtained by forming the ratio

$$R(t) = 2[C(180,t)-C(90,t)]/[C(180,t)+2C(90,t)] \quad (4)$$

where $C(\theta, t)$ is proportional to $W(\theta, t)$ and $C(90, t)$ and $C(180, t)$ are the coincidence counting rates measured at time t with angles between detectors of 90° (or 270°) and 180°, respectively.

For the determination of the hyperfine parameters ω_Q, η and δ, least-squares fit of Eq. (2) to the experimental results (Eq. (4)) was performed.

For the measurement of the angular correlation spectra as a function of temperature the samples were heated in-situ in a furnace with a thermal stability better than 1 °C. For each composition the measurements were made so as to explore the EFG above and below T_C.

5. Results

For the three compositions studied two static, asymmetric and disordered electric quadrupole interactions at the ^{181}Ta PAC probe were fitted to the obtained spectra. In all cases, one of them is by far the most populated ($f > 95\%$), and the corresponding V_{zz} values are between the typical values observed for other perovskite-type compounds. The other one is characterized by very high V_{zz} values which are outside the expected range obtained in previous PAC studies done in perovskites that display different cell symmetries and by computational simulations [18–25]. Thus, in what follows we will refer only to the highly populated site, being the other one in principle related with some kind of defect, grain boundaries or surface effects.

After the maximum temperature was reached, a final spectrum at RT was taken and compared with the initial measurement for the three compositions. No changes were observed in the corresponding hyperfine parameters, thus indicating that no irreversible changes due to the thermal process occurred.

For the spectra fit, when the asymmetry parameter resulted close to 1 or 0 it was fixed at the obtained values in order to calculate the error bars of the other hyperfine parameters and fraction.

a) $PbTi_{0.25}Hf_{0.75}O_3$

In Fig. 2 some spin precession curves for this composition above and below T_C are shown. Measurements were performed up to 300 °C. In Fig. 3 the hyperfine parameters ω_Q, η and δ as a function of temperature obtained from the fits of Eqs. (2)–(4) to the experimental data can be observed. The fitted hyperfine parameters at RT are: $\omega_Q=85(2)$ Mrad/s, $\eta=0.41(5)$ and $\delta=60(2)\%$. For this Ti concentration, previous studies [12–13] reported that the compound is in a rhombohedral Pbam ferroelectric phase from RT to about 270 °C (T_C), and in a cubic Pm3m paraelectric phase above this temperature. In the figure it can be seen that between 200 °C and 220 °C, the hyperfine parameters present an abrupt change, which should correspond to the previously reported first order phase transition but at a lower temperature. From RT to T_C, ω_Q grows slowly from 85 to 120 Mrad/s. The asymmetry parameter remains almost constant with a value of 0.40, and the distribution width parameter present high values, about 70%, indicating the presence of disorder in the sample. Above T_C, ω_Q falls sharply to a value of about 70 Mrads/s, the asymmetry parameter drops to zero, and the distribution falls down to a value of about 30–40%. All the hyperfine parameters remain almost constant in the measured

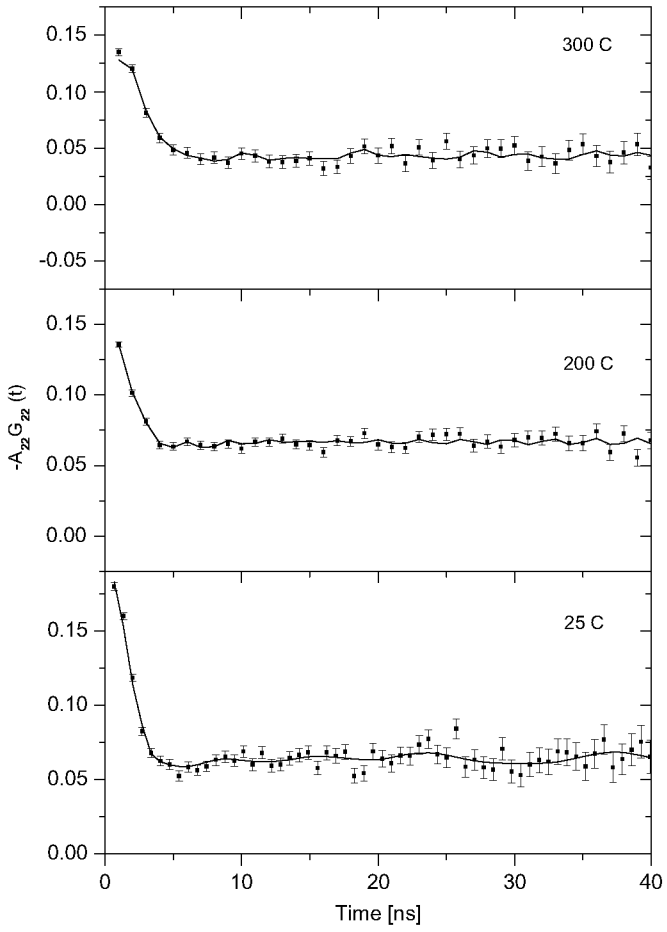

Fig. 2. PAC spectra of $PbTi_{0.25}Hf_{0.75}O_3$ measured at different temperatures above and below T_C.

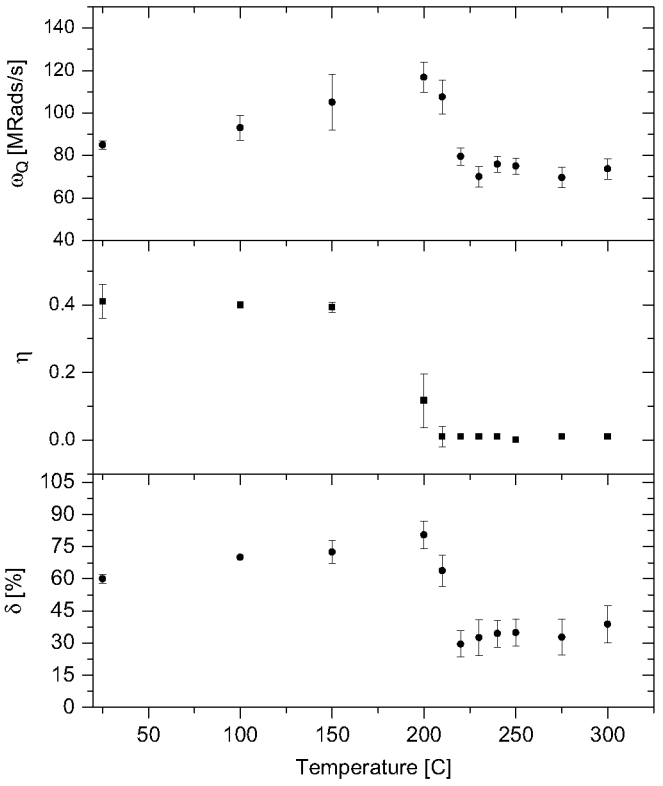

Fig. 3. Hyperfine parameters ω_Q, η and δ as a function of temperature for $PbTi_{0.25}Hf_{0.75}O_3$.

temperature range above T_C. It can be observed that the phase transition produces an internal ordering of the sample indicated by the reduction of the distribution width. By symmetry in the cubic Pm3m phase, both ω_Q and η should be null. Nevertheless, in this phase a zero value for the EFG at Ta PAC probes for other $ABB'O_3$ perovskite-type compounds was never observed [22]. The remaining value of V_{zz} in the cubic phase has been related with the disorder introduced in the B–B′ sites of the samples due to the different B and B′ electronic configurations, different O–B(B′)–O distances, and the local distortion of the structure around the Ta site which acts as an impurity and has an extra electron compared with the Hf host atom. The disorder in the B–B′ site, is related with the random distribution of B and B′ specimens in the lattice. In this case, random distributions of Ti and Hf in the corresponding proportions occupying the central site of the perovskite. Ti and Hf have both the same 4+ valence, but they have different ionic radii, and different electronic configurations. So, the Ti–O bonds and the Hf–O bonds should have different distances, thus producing random local distortions. Due to this, the cubic phase in a $A(BB')O_3$ perovskite must be understood as a "mean cubic phase", because the lattice is locally distorted at random due to the re-accommodation of each unit cell depending on the specimens in the neighbor cells. On the other hand, the presence of the Ta probes produces other local distortions, also related with its own ionic radius and electronic configuration, different to those of Ti and Hf. Although the sample has few distortions of this kind due to the ppm proportion of the Ta PAC probe, the PAC measurements are done at the Ta sites, thus every count in the detectors comes from a locally distorted Ta site, which in turn have the surrounding cells distorted by the (BB′)–O random distribution. These are the reasons why albeit in an ideal ABO_3 cubic perovskite the EFG should be null in the B site, in a Ta doped ABO_3 perovskite the EFG in principle will not be null, and even less in a Ta-doped $ABB'O_3$. Both the doping and the disorder in the B–B′ site contribute to a no-null EFG in the cubic phase, and the corresponding distribution line width. The B–B′ disorder also produces the high frequency spread reflected in the high δ values that were observed in various $ABB'O_3$ perovskites.

b) $PbTi_{0.50}H_{0.50}O_3$

In Fig. 4, the fitted values of the hyperfine parameters for $PbTi_{0.50}Hf_{0.50}O_3$ are shown. Measurements were performed up to 375 °C. The corresponding values for RT are: $\omega_Q = 78(2)$ Mrad/s, $\eta = 0.41(6)$ and $\delta = 60(4)\%$. Between 300° C and 320° C a change can be observed in the trend of ω_Q, η and δ that should correspond to the first order phase transition previously reported at about 357° C. Below this temperature (T_C), ω_Q diminishes slowly, and changes from about 78 Mrad/s to about 64 Mrad/s at T_C. Above this temperature in the cubic phase ω_Q remains almost constant. The main unexpected fact occurs for η and δ. The asymmetry parameter η jumps from a value about 0.40 below Tc, to nearly 1 above T_C, contrary to what occurred in the previous composition. Also, δ jumps from values around 60% below T_C (which reflects a high degree of disorder in the sample) to even higher values at about 100% above T_C, indicating a major disorder around the probes. The high value of η indicates a high local asymmetry around the probe atom ^{181}Ta ($V_{XX} \approx 0$) characteristic of lower symmetry B cations arrangements. But, as it was already mentioned for the previous composition, null values for V_{ZZ} in the cubic phases were not observed in $ABB'O_3$ compounds, due to the presence of disorder. In this sample, the increment in the δ parameter shows that in the high temperature phase the disorder is significant, which should justify the strange behavior of the η, together with the finite value of V_{ZZ}. As it was pointed

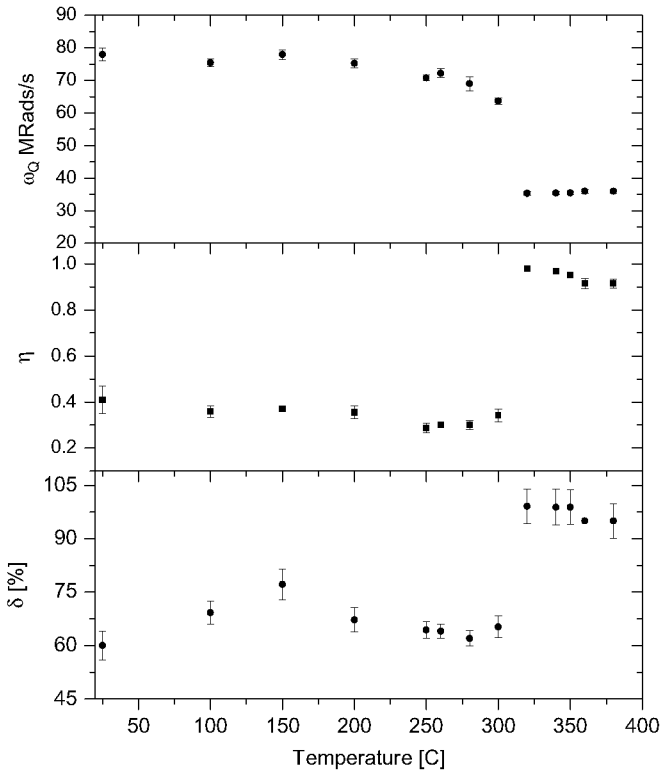

Fig. 4. Hyperfine parameters ω_Q, η and δ as a function of temperature for $PbTi_{0.50}Hf_{0.50}O_3$.

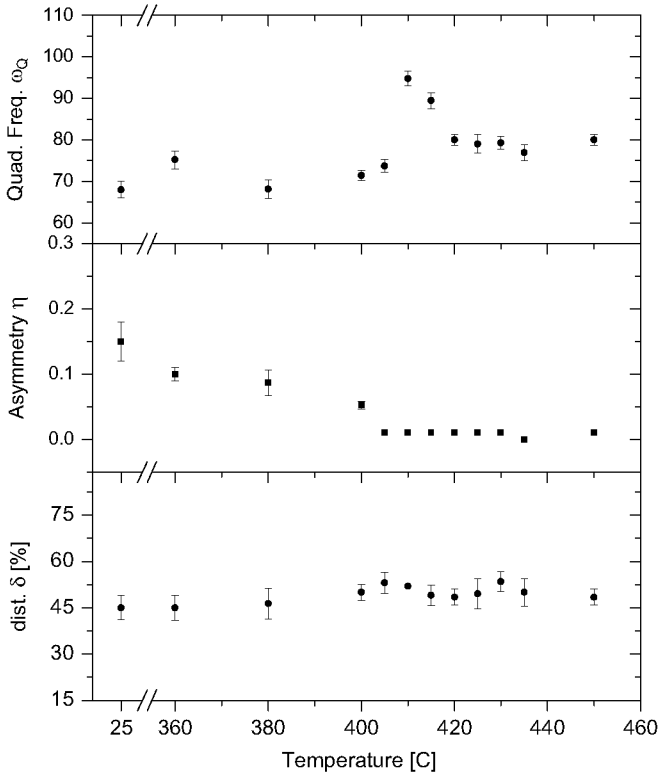

Fig. 5. Hyperfine parameters ω_Q, η and δ as a function of temperature for $PbTi_{0.75}Hf_{0.25}O_3$.

out previously this composition lies on the morphotropic phase transition, where tetragonal, monoclinic and rhombohedral structures can coexist at low temperatures [14,30]. Our results show that above T_C, a high degree of disorder remains up to about 375 °C.

c) $PbTi_{0.75}Hf_{0.25}O_3$

For this composition the hyperfine parameters obtained after the data fit are shown in Fig. 5. Measurements were performed up to 450 °C. The obtained values of the hyperfine parameters at RT are ω_Q=68(2) Mrad/s, η=0.15(3) and δ=45(4)%, and the compound is in the tetragonal phase. This fact is reflected in the asymmetry parameter that is lower for this composition than for the previous ones. In a perfect sample, η should be zero (provided ω_Q is not null). In the figure a discontinuity in the hyperfine parameters between 400 °C and 415 °C which should correspond to the ferroelectric–paraelectric phase transition previously reported at 420 °C can also be observed [13]. The quadrupole frequency shows a nearly constant behavior below T_C at about 70 Mrad/s. At T_C it jumps to higher values and then diminishes to a lower and nearly constant value of about 80 Mrads/s. At T_C, the asymmetry parameter goes to zero and remains null above T_C indicating that probes are in an axially symmetric sites. The distribution parameter remains almost constant below and above T_C, showing that the disorder level is mainly not altered in the phase transition.

6. Discussion

Previous PAC studies in PH revealed that the two antiferroelectric phases are characterized with the following hyperfine parameters: at RT ω_Q=46.8(4) Mrad/s, η=0.80(2) and δ=7.0(3)% [31]. These parameters are almost temperature independent. Above T_{C1} the intermediate phase is characterized by ω_Q=35(3) Mrad/s, η=0.7(1) and δ=45(5)%. In PT at RT the hyperfine parameters are ω_Q=125(5) Mrad/s, η=0.61(6) and δ=11(2)% [32]. The quadrupole frequency depends on temperature but η and δ are nearly temperature independent. In the respective cubic phases of these oxides at temperatures above $T_{C2} \approx 210$ °C in PH and above $T_C \approx 490$ °C in PT the hyperfine perturbation are characterized by weak interactions that are produced by defects.

For the three $PbTi_{1-x}Hf_xO_3$ compounds studied in the present PAC work, lower T_C values as compared with those previously obtained by other techniques were found. Especially for the x=0.75 composition. The PAC measurements were done using the samples that were used previously for the Impedance Spectroscopy (IS) experiments [13]. But, the samples suffer different modifications for PAC spectroscopy: (a) samples used for IS are in the form of pressed pellets. Then, for PAC measurements the contacts were removed and the samples were ground to obtain a fine powder. (b) the samples were then send to a branch of a nuclear reactor to be irradiated by a flux of thermal neutrons to obtain the 181Ta PAC probe form the already contained in the samples 180 Hf. Based on previous experience in similar compounds, we do not expect that the irradiation damage during the activation process nor the presence of the probe itself in as low as ppm proportion can produce measurable changes in the temperature of the phase transitions of the samples. (c) each PAC spectrum lasts 24–30 h. Thus, the samples undergo a long heat treatment during the measurements. For example, to reach the 400 C point in the x=0.50 sample, the sample has suffered an ascending heat treatment of more than 15 days. Each measurement in IS spectroscopy lasts 2–3 min, thus by comparing the typical time of both techniques, we cannot say anymore that these have the same samples. During PAC measurements the samples can undergo modifications. But, there is another major difference. In the IS work, there are shown results obtained by IS and DSC, which are fundamentally

macroscopic analysis of bulk samples. In the present work we use PAC spectroscopy which is sensible to local variations at a nanoscopic level. We cannot know a priori if there is a nanoscopic process that begins at lower temperatures, as nucleus of formation of the cubic phase that will propagate along the whole samples, or the thermal treatment affected the samples in a way to stabilize the cubic phase at lower temperatures. Also, may be that the transition to the cubic phase be made via some intermediate phase, as the reported monoclinic phase for $x=0.50$. The obtained line width distribution do not enable us to resolve the presence of more than one phase, as explained below. New and targeted studies are needed to clarify this important question. Depending on its applications this fact must be taken into account for the expected behavior of the material.

The electronic configurations of the Ti and Hf atoms are quite different: Ti has $[Ar]3d^25s^2$ states and Hf has $[Xe]4f^{14}5d^26s^2$ states. In the 4+ state both have closed shell structure. The electronic configuration of Pb and O atoms are $[Xe]6s^24f^{14}5d^{10}6p^2$ and $[He]2s^22p^4$ and also have closed shell structure for the valence values of 2+ and 2−, respectively. Bonds between ions can be either ionic or covalent depending on the sum of the ionic radii and on the ion–ion distances. Assuming that these distances in PT and PH pseudo cubic structures can be deduced from the corresponding lattice constants results that $\langle a(PT)\rangle=3.992$ Å and $\langle a(PH)\rangle=4.052$ Å being $\langle a\rangle$ the pseudocubic lattice constant. By summing the corresponding ionic radius of Ti, Hf, Pb and O results in $r_{(Ti+Pb)}=2.095$ Å, $r_{(Ti+O)}=1.955$ Å, $r_{(Hf+Pb)}=2.20$ Å and $r_{(Hf+O)}=2.06$ Å, respectively. When these quantities are compared with cation–cation and anion–cation distances it arises that Pb–O bond in PT and Hf–O bond in PH are covalent while the rest of bonds in PT and PH are ionic. The electron distribution in PT is different to that of PH and while Ti concentration increases replacing Hf in the solid solution there is a change in the electronic distribution in the unit cell because the charge transfers between cations and between cations and oxygen atoms. Charge with $3d^25s^2$-structure is added and charge with $5d^26s^2$-configuration is taken away and this charge transfer will produce changes in all properties of the solid solution. The EFG at probe positions depends on the electron distribution at these sites and on the r^{-3} factor. As this distribution is random the EFG is represented by the mean value of the quadrupole frequency ω_Q, asymmetry parameter η and by the line width δ. The EFG at probes in the B–B′ site is mainly produced by d electrons from Ti and Hf and p electrons from O. The p contribution to the EFG is not weak due to the r^{-3} factor.

In agreement with previously reported results the three mixtures studied by PAC only show one phase transition in the observed temperature range and it is observed that the T_C depends linearly on composition. PH also has a second phase transition at $T_{C1}=165$ °C that is not observed in PTH even at low Ti concentrations ($x=0.25$).

For $x\approx 0.75$, the behavior of the hyperfine parameters with temperature below and above T_C is what should be expected in perovskites: a jump to lower values of ω_Q and η at T_C. The remaining finite value for V_{zz} above T_C is associated with the presence of defects, mainly Ti and Hf at random lattice B and B′ sites, and O or Pb vacancies. In the cubic phase the null value of η indicates that the Z-axis is a symmetry axis. The line width in the tetragonal phase is double the corresponding value in the cubic structure, indicating a higher degree of disorder in the structure with lower symmetry.

According to previous structural studies, in the morphotropic region ($0.45\le x\le 0.5$), the sample contains variable amounts of coexisting tetragonal, monoclinic and rhombohedral phases [14,30]. The monoclinic intermediate phase would result from small Pb cation random shift from tetragonal ideal sites. These displacements promote the transition from tetragonal to monoclinic structure. The distances between O and B or B′ chains O–B(B′)–O along the crystallographic axis depend on composition and as the substitution of B by B′ is random these distances are also random. This means that the oxygen octahedral is distorted and the electron distribution is a random mixture of s, p and d orbitals from O, Pb, Ti and Hf. This scenario should correspond with different sites to the ^{181}Ta probe, each one related with one of the coexisting symmetries. According to this, attempts to fit the spectra with more sites were done. The resulting fits were not better, compared with the previous ones containing only one site for the low frequency electric quadrupolar interaction. As it was mentioned in the introduction of this work, in perovskite-type compounds the phase transitions occurs via different very tiny deformations of the cubic cell. Taking this fact into account, it is possible that the EFG in the probe atom for the tetragonal, monoclinic or rhombohedral phases that coexist in the morphotropic region be similar in magnitude. In that case, the fit will be reasonably good with only one average interaction and a relatively high δ parameter that takes into account the spread due to the different symmetries present. Moreover, in the present case the δ parameter is already high due to the local disorder in the BB′ arrangement. Thus, the presence or absence of different phases below T_C cannot be resolved with the obtained spectra. It should be noted that above T_C, the disorder (δ) augments. And that this fact only occurs for the composition belonging to the morphotropic region. The EFG for this composition only has one component perpendicular to V_{ZZ}, the other is null ($\eta=1$). In the previous analysis, the disorder was associated with the B–B′ random distribution and with the presence of vacancies. But none of these components is expected to augment in a transition to a cubic symmetry. Moreover, the normal situation is similar to that of the $x=0.25$ composition, in which the disorder diminishes by transforming to the cubic phase. Thus, the observed jump in the distribution width parameter in the cubic phase indicates the existence of more complex physical behavior, which may be directly related with the different coexisting symmetries that exist below T_C.

The temperature dependence of the hyperfine parameters in the Ti richest solid solution displays a striking effect in the phase transition from rhombohedral to cubic lattice in the peak of $\omega_Q(T)$.

7. Conclusions

In this work the hyperfine interactions as a function of temperature of $PbTi_{1-x}Hf_xO_3$ for $x=0.25$, 0.50 and 0.75 using PAC spectroscopy with ^{181}Ta probes were analyzed. In each sample two static and disordered electric quadrupole interactions were observed. The most abundant site (>0.95) corresponds to probes in the B–B′ sites of the perovskite, and the other one should be related with defects. The phase transition from ferroelectric to paraelectric is observed and a nanoscopic description is provided. The temperatures of the transition to the cubic phase increases as x decreases. In this work they were observed at lower temperatures than previously reported. For the $x=0.50$ composition, which corresponds to the morphotropic phase transition, an abnormal behavior is observed for the asymmetry and distribution width parameters in the transition to the cubic phase. Both parameters augment above T_C, indicating the presence of some complex process that may be related with the coexistence of different phases below T_C.

Acknowledgments

This work was partially supported by CONICET and the University of La Plata.

References

[1] C.J. Howard, K.S. Knight, B.J. Kennedy, E.H. Kisi, J. Phys.: Condens. Matter 12 (2000) 677.
[2] R.E. Alonso, J. de Frutos, M.A. de la Rubia, M. Taylor, A.R. López-Garcia, Bol. Soc. Esp. Ceram. Vidrio 46 (2007) 311.
[3] G. Xu, H. Luo, Z. Yin, Phys. Rev. B 64 (2001) 020102.
[4] M. Glerup, K.S. Knight, F.W. Poulsen, Mater. Res. Bull. 40 (2004) 507.
[5] C.J. Howard, H.T. Stokesc, Phase Transitions 61 (2005) 93.
[6] P.M. Woodward, Acta Crystallogra. B53 (1997) 32.
[7] M.A. Bunin, S.A. Prosandeyev, I.I. Gegusin, I.M. Tennenboum, Radiat. Eff. Defects Solids 134 (1996) 75;
M.V. Raymond, D.M. Smyth, J. Phys. Chem. Solids 57 (1996) 1507;
W.L. Warren, K. Vanheusden, D. Dimos, G.E. Pike, B.A. Tuttle, J. Am. Ceram. Soc. 79 (1996) 536;
G.V. Lewis, C.R.A. Catlow, J. Phys. Chem. Solids 47 (1986) 89.
[8] A.M. Glazer, S.A. Mabud., Acta Crystallogra. B34 (1978) 1065.
[9] A. Sani, M. Hanfland, D. Levy, J. Solid State Chem. 167 (2002) 446.
[10] J. Kwapulinski, M. Pawelczyk, J. Dec, J. Phys.: Condens. Matter 6 (1994) 4655.
[11] Y. Kuroiwa, H. Fujiwara, A. Sawada, S. Aoyagi, E. Nishibori, M. Sakata, M. Takata, H. Kawaji, T. Atake, Jpn. J. Appl. Phys. 43 (2004) 6799.
[12] B. Jaffe, R.S. Roth, S. Marzullo, J. Res. Nat. Bur. Stand. 55 (1955) 239.
[13] M.A. de la Rubia, R.E. Alonso, A. López García, J. de Frutos, J. Therm. Anal. Calorim. 98 (2009) 793.
[14] J. Frantti, Y. Fujioka, S. Eriksson, S. Hull, M. Kakihana, Inorg. Chem. 44 (2005) 9267.
[15] C. Bedoya, C. Muller, J.L. Baudour, F. Bouree, J.L. Soubeyroux, M. Roubin, J. Phys.: Condens. Matter 13 (2001) 6453.
[16] C. Muller, J.L. Baudour, V. Madigou, F. Bouree, J.M. Kiat, C. Favotto, M. Roubin, Acta Crystallogra. B55 (1999) 8.
[17] N. Sicron, E. Stern, Y. Yacoby, J. Phys. Chem. Solids 61 (2000) 243.
[18] R.E. Alonso, P. de la Presa, A. Ayala, A. López García, J. Phys.: Condens. Matter 10 (1998) 2139.
[19] R.E. Alonso, P. de la Presa, A. Ayala, A. López García, J. Korean Phys. Soc. 32 (1998) S634.
[20] P. de la Presa, R.E. Alonso, A. Ayala, V.V. Krishnamurthy, K.P. Lieb, A. López García, M. Neubauer, M. Uhrmacher, J. Phys. Chem. Solids 60 (1999) 749.
[21] A. López García, R.E. Alonso, P. de la Presa, A. Ayala, Hyp. Interact. 120/121 (1999) 97.
[22] R.E. Alonso, A. López-García, Z. Naturforsch. 55a (2006) 261.
[23] R.E. Alonso, A.P. Ayala, P. de la Presa, C. Horowitz, A. López-García, Ferroelectrics 274 (2002) 17.
[24] A. López-García, R.E. Alonso, J. Phys.: Condens. Matter 17 (2005) 7717.
[25] A. Lopez-García, P. de la Presa, Phys. Rev. B 44 (1991) 9708.
[26] T. Butz, S.K. Das, Y. Manzhur, Z. Naturforsch. 63a (1) (2008).
[27] R.E. Alonso, L.A. Errico, E.L. Peltzer y Blanća, A. López-García, A. Svane, N.E. Christensen, Phys. Rev. B 78 (2008) 1;
M.A. Taylor, R.E. Alonso, L.A. Errico, A. López-García, P. de la Presa, A. Svane, N.E. Christensen, Phys. Rev. B 82 (2010) 165203;
M. Rentería, G.N. Darriba, L.A. Errico, E.L. Muñoz y, P.D. Eversheim, Physica Status Solidi B 242 (2005) 1928;
G.N. Darriba, L.A. Errico, P.D. Eversheim, G. Fabricius, M. Rentería., Phys. Rev. B 79 (2009) 115213;
G.N. Darriba, L.A. Errico, E.L. Muñoz, D. Richard, P.D. Eversheim, M. Rentería, Physica B 404 (2009) 2739.
[28] R. Beraud, I. Berkes, J. Daniere, G. Marest, R. Rouguy, Nucl. Instrum. Methods 69 (1969) 41;
G.L. Catchen, L.H. Menke Jr., K. Jamil, M. Blaszkiewicz, B.E. Scheetz, Phys. Rev. B 39 (1989) 3826;
H. Frauenfelder, R.M. Steffen, Alpha-, Beta- and Gamma-Ray Spectroscopy, K Siegbahn (Ed.), Amsterdam, 1965.
[29] T. Butz, A. Lerf, Phys. Lett. 97A (1983) 217.
[30] L. Bellaiche, A. García, D. Vanderbilt, Phys. Rev. Lett. 84 (2000) 5427.
[31] M. Forker, A. Hammesfahr, A. López-García, B. Wolbeck, Phys. Rev. B 7 (1973) 1039.
[32] G.L. Catchen, S.J. Wukitch, D.M. Spaar, M. Blaszkiewics, Phys. Rev. B 42 (1990) 1885.